# Postflame Reaction Chemistry of Dichloromethane: Variations in Equivalence Ratio and Temperature

**L. A. SGRO, C. P. KOSHLAND,* D. LUCAS, and R. F. SAWYER**

*Department of Mechanical Engineering, School of Public Health, Lawrence Berkeley National Laboratory, University of California-Berkeley, Berkeley, CA 94720, USA*

We report on the destruction pathways and byproduct formation of dichloromethane ($CH_2Cl_2$) in conditions typical of incinerator postflame regions (injection temperature = 900–1200 K; equivalence ratio = 0.6, 0.9, 1.0, 1.1; residence time = 0.28–0.35 s). This is the first study to independently vary equivalence ratio and temperature, and evaluate their impacts on byproduct yield and destruction efficiency. We inject 750 ppm $CH_2Cl_2$ into postflame combustion products and measure byproducts with extractive FTIR spectroscopy. We use a detailed chemical kinetic mechanism and reaction rate analysis to predict the changes in reaction pathways as a function of equivalence ratio. The predictions for major products and several intermediate species compare well with experiments; the largest disparities are an underprediction of phosgene ($CCl_2O$) and an overprediction of methyl chloride ($CH_3Cl$). Both the experiment and the numerical predictions show increased destruction at lower equivalence ratios. However, the experiments reveal increased levels of stable chlorinated organics at lower equivalence ratios, opposite to the numerical prediction. We discuss reasons for this discrepancy and implications of these results for designing control strategies to promote full conversion to HCl and to reduce chlorinated byproduct emissions. 

## INTRODUCTION

Incineration of chlorinated hydrocarbons (CHCs) is seen as a preferable disposal option compared to storage in landfills because very high destruction efficiencies (99.99%) reduce future risk of exposure. The primary drawback to incineration is the formation and possible emission of even low levels of toxic byproducts—essentially any chlorinated species other than the desired hydrochloric acid (HCl). Chlorinated byproducts or products of incomplete combustion (PICs) are the organic species of greatest concern for public health because of their high toxicity and persistence in the atmosphere [1–3]. The major cause of CHC emissions in incinerators is thought to be off-design or upset conditions that cause chlorinated waste fuel to escape the flame zone and react in postflame conditions where insufficient oxygen, radicals, or residence time at high temperatures prohibits complete conversion of chlorine to HCl [4–8].

It is important to understand the chemical destruction pathways of CHCs with sufficient detail to reliably predict stable chlorinated PICs to improve their control and reduce potential exposures. Because human health effects depend strongly on chemical structure, the toxicity of emissions changes nonlinearly as CHC waste is converted to intermediate species and HCl. Chlorinated PICs can interact with toxic metals in incinerators, increasing their vapor pressure and emission potential [9]. Conditions in which chlorinated PICs persist undermine control strategies by delivering sources of chlorine other than HCl to low temperature regions, where *de novo* synthesis of dioxins and furans can occur [10].

## LITERATURE REVIEW

Recent years have witnessed considerable progress in understanding the combustion chemistry of $C_1$ and $C_2$ CHC decomposition using flat flames [5, 11, 12], isothermal flow reactors [4, 13–18], combustion-driven flow reactors [4, 19–23], and through the development of chemical kinetic mechanisms [13, 24]. However, the destruction of CHCs and byproduct formation in postflame conditions is not presently well understood. Previous $CH_2Cl_2$ flame and flow reactor studies have drawn widely varying conclusions with respect to effects of equivalence ratio: some investigators find that changing equivalence ratio does not vary the

*Corresponding author. E-mail: ckosh@uclink4.berkeley.edu

0010-2180/00/$–see front matter
PII S0010-2180(99)00119-4

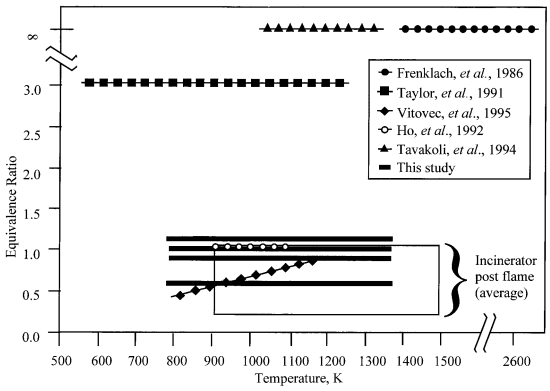


Fig. 1. Incinerator postflame conditions compared with conditions of $CH_2Cl_2$ flow reactor studies. This work presents the first systematic study of the impacts of equivalence ratio and temperature on byproduct formation for conditions modeling the postflame region of industrial incinerators.

chemistry significantly [17], others find that increasing the equivalence ratio increases the amount and number of byproducts [16], and yet others find that increasing the equivalence ratio decreases the amount of byproducts [11, 25].

Most flow reactor studies consider a single equivalence ratio while varying temperature [4, 13–18]. No study systematically examines changes in $CH_2Cl_2$ destruction and byproduct formation by independently varying equivalence ratio and temperature in postflame conditions. While the equivalence ratio of most incinerators is fuel-lean (~0.3–1.0), previous studies typically probe high equivalence ratio conditions as the worst-case scenario, arguing that high equivalence ratio and pyrolysis conditions inhibit destruction of $CH_2Cl_2$ while promoting the formation of higher molecular weight species. Figure 1 illustrates the operating conditions of reviewed flow reactor studies, the average postflame conditions of incinerators [26], and the conditions examined in this study.

Ho et al. [13] show how changes in equivalence ratio affect the global conversion process (i.e., destruction of $CH_2Cl_2$, HCl formation, and CO to $CO_2$ conversion), but they discuss byproduct formation and destruction for only one equivalence ratio ($\Phi = 1.0$). Vitovec et al. [4] examine byproduct formation from $CH_2Cl_2$ in lean postflame conditions, but without independent control over temperature and equivalence ratio. Taylor and Dellinger [16] compare pyrolytic to highly oxidative ($\Phi = 0.05$) conditions in a flow reactor, injecting mixtures of $CH_2Cl_2$ and other chlorinated methanes. They conclude that the number and yield of PICs are greater in pyrolytic conditions. In another study by the same authors [17], the effects of oxygen are evaluated in two flow reactor studies at pyrolytic and oxidative pyrolytic conditions ($\Phi = 3.0$); similar product yields led the authors to conclude that oxygen does not affect the chemistry, except to reduce the formation of nonperchlorinated products.

A comparison of the fuel-rich $CH_2Cl_2/CH_4/Ar/O_2$ flames ($\Phi = 2.15$ and 1.9) of Qun and Senkan [11] and the lean $CH_2Cl_2/CH_4$/air flame ($\Phi = 0.8$) of Senser et al. [12] shows that rich flames produce more diverse byproducts [11]. Cundy et al. [25] vary equivalence ratio ($\Phi = 0.8, 1.0, 1.1$) in a flat flame and conclude that the destruction levels of $CH_2Cl_2$ and PICs are slightly enhanced in the higher equivalence ratio flames.

## EXPERIMENTAL APPARATUS

Gas-phase $CH_2Cl_2$ is injected into a transitional to turbulent flow of combustion products from $CH_4$/air flames with a temperature gradient similar to those reported in the postflame region of incinerators [26]. Independent control of equivalence ratio and temperature is achieved by mixing cooled products of an external $CH_4$/air flame with hot products from an internal flame [27]. The two flames operate with identical equivalence ratios. We adjust the temperature by varying the flow of cooled and hot combustion products while maintaining a constant total flow rate. The equivalence ratio is changed by adjusting the fuel/air ratio, or by adding secondary air upstream of the $CH_2Cl_2$ injection (Fig. 2).

$CH_2Cl_2$ is vaporized in a flow of $N_2$ comprising 2% of the total flow. The injector is water-cooled to minimize $CH_2Cl_2$ reactions prior to injection into the combustion products flow. The concentration of the injected $CH_2Cl_2$ in the flow reactor is held constant at 750 ppm. $CH_4$, air, and $N_2$ flows are controlled by calibrated Teledyne-Hastings 0–500 slpm mass flow controllers. The uncertainty in these meters is less

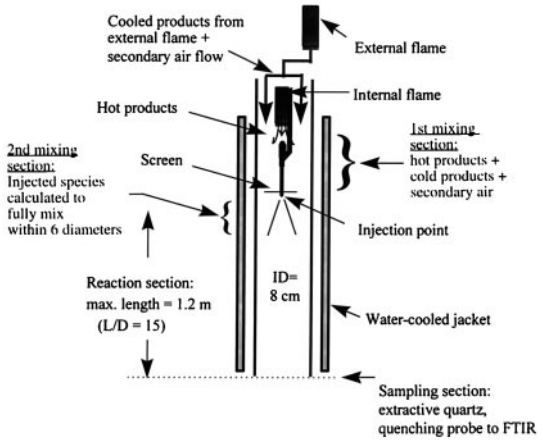


Fig. 2. Combustion-driven flow reactor. By varying the relative amount of cooled products from the external flame and hot products from the internal flame, we control the temperature profile in the reaction section independent of equivalence ratio.

than 5%, which leads to an uncertainty in the equivalence ratios of $\pm 0.1$. Experimental measurements are plotted against the temperature at the point of injection ($T_{inj}$), obtained from measured data taken with a type K thermocouple.

A decreasing temperature gradient of about 500 K/s (similar to those reported typical of incinerator postflame zones [28]) exists in the reaction zone. The experiments have been modified to reduce radial nonuniformities. In the highest temperature experiments, radial nonuniformities are calculated to persist for 6 diameters, but measurements of injected NO, which does not react at these temperatures, shows uniform profiles after 4 diameters [27, 29]. For lower temperature experiments, the profiles become uniform (within 5%) after 1–2 diameters. Samples are taken at ~15 diameters downstream of injection in the coolest portion of the flow, well downstream of where the majority of the chemical reactions occur.

Species are sampled through a 3-mm diameter quartz suction probe, operating at approximately 0.1 atm at a point 1.2 m downstream of CHC injection. The sample is drawn through a White cell with a total path length of 13.68 m, and quantified using a Biorad FTS-40 Fourier transform infrared (FTIR) spectrometer. Each sample flows through the cell for 40 minutes at a pressure of 35 or 71 Torr to equilibrate HCl wall adsorption. CHCs are readily quantified using FTIR spectroscopy since the C–Cl stretching region (500–750 $cm^{-1}$) is relatively free of $CO_2$ and $H_2O$ absorption [30]. We average 64 scans per sample with a total scanning time of approximately 6 minutes. The lower limit of detection for most species is between 1–10 ppm. While the systematic error on the absolute concentration measurement is approximately 20% [31], the relative error between measurements under identical conditions is 1–5%. $O_2$, $CO_2$, and $H_2O$ concentrations in the $CH_4$/air combustion products are high ($\sim 10^5$ ppm) relative to the concentration of $CH_2Cl_2$ injected (750 ppm), and we do not attempt to quantify the small differences in these species. At a cell pressure of 71 Torr, the chlorine mass balance decreased as a function of temperature, but we observed unexpected condensation in the cell and sample lines for the highest temperature and equivalence ratio experiments. Reducing the cell pressure to 35 Torr eliminated condensation for all of the experimental conditions, and only the HCl concentrations increased. The chlorine balances at lower cell pressure show that the various measured byproducts reported account for the chlorine initially input into the reactor as gas-phase $CH_2Cl_2$.

## NUMERICAL MODELING

Reactions are modeled assuming plug flow [31] with the CHEMKIN equation solver package [33]. Measured centerline temperatures are used, eliminating the need to simultaneously solve heat and mass transport equations. The concentrations of all $CH_4$–air combustion products at the point of injection except for CO are calculated assuming equilibrium for a given equivalence ratio and injection temperature, and entered as initial species concentrations in the numerical simulations. The initial CO concentration is set to the measured value for each run, which is slightly higher than equilibrium predictions at the temperature near the point of injection. The initial concentration of $CH_2Cl_2$ is 750 ppm for all simulations.

Calculating an exact residence time from axial distance is a common problem in all flow reactor studies because injected species require

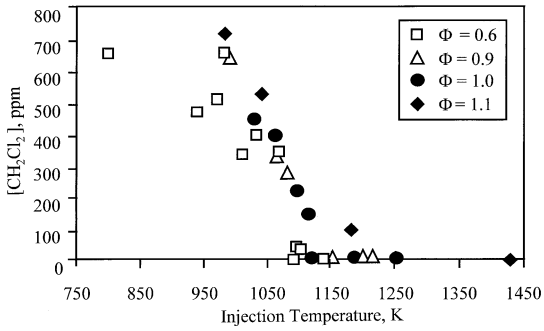


Fig. 3. Dichloromethane ($CH_2Cl_2$) concentration, residence time ≈ 300 ms. We inject 700 ppm into postflame conditions while varying injection temperature and equivalence ratio. The overall destruction of $CH_2Cl_2$ is enhanced in low equivalence ratio conditions.

time to mix with the bulk flow. We calculate residence time as a function of measured centerline temperature and measured inlet ambient temperature mass flow rates for each experiment. The measured temperature and calculated residence time are input to the numerical model. We later discuss the relative ability of the model to predict measured stable species as a function of temperature and equivalence ratio, since uncertainties exist in calculating residence time in the first few diameters when the flow is not fully mixed. Results are presented at relatively long residence times, corresponding to 294 ms for the highest temperature profiles and 234 ms for the coolest temperature experiments.

The chemical mechanism used was first developed and reported by Ho et al. [13, 33, 34], and recently modified to include the addition of more destruction reactions for the $C_2$-species [35, 36]. The mechanism contains 440 reactions and 120 species. None of the rate parameters or reactions in the mechanism is modified to fit our experimental data.

## EXPERIMENTAL RESULTS

### Major Species

Figure 3 shows the measured concentration of $CH_2Cl_2$ at various equivalence ratios as a function of injection temperature. Increasing the equivalence ratio raises the temperature required to achieve a given level of destruction, consistent with the observations of Ho et al. [13]. $CH_2Cl_2$ destruction begins at lower injection temperatures for fuel-lean conditions with the greatest change between $\Phi = 1.0$ and 1.1. HCl production also requires higher injection temperatures as equivalence ratio increases.

CO from $CH_2Cl_2$ destruction is of the order 10 ppm for $\Phi = 0.6$, 100 ppm for $\Phi = 0.9$ and 1.0, and $10^4$ ppm for $\Phi = 1.1$. Peak CO concentrations are detected at the same injection temperature required to fully destroy injected $CH_2Cl_2$. At higher injection temperatures, CO returns to equilibrium levels expected for methane/air combustion products without $CH_2Cl_2$ injection. This is consistent with a two-stage CHC combustion process of fast CHC reactions to form CO and intermediate species, followed by a slower, chlorine-inhibited CO to $CO_2$ burnout [13, 37–40].

At similar temperatures, as the equivalence ratio increases, $CH_2Cl_2$ destruction and HCl formation decrease, while the concentration of CO increases. This indicates that higher equivalence ratios decrease the conversion of $CH_2Cl_2$ to the desired products HCl, $CO_2$, and $H_2O$. The elevated CO concentrations suggest chlorine inhibition by radical scavenging, with inhibition more pronounced at higher equivalence ratios. Examining only the major species supports the theory that fuel-rich environments are the worst conditions for burning CHCs, since less chlorine is converted to the desired HCl.

### Intermediate Species

Table 1 summarizes the stable intermediates detected. While more $CH_2Cl_2$ is destroyed, experiments with lower equivalence ratios produce higher concentrations of chlorinated ethene species and phosgene ($CCl_2O$). $CCl_2O$ is the most abundant of the intermediate species. Its concentration is highest in the leanest experiments ($\Phi = 0.6$), accounting for 15% of the chlorine from the injected $CH_2Cl_2$, while no $CCl_2O$ is detected for the richest experiments ($\Phi = 1.1$) (Fig. 4). The peak $CCl_2O$ concentration strongly depends on equivalence ratio, but the temperature at which it peaks remains constant at $T_{inj} \sim 1100$ K (Fig. 4). The only other study that reported detection of $CCl_2O$ from $CH_2Cl_2$ combustion was also conducted in our

**TABLE 1**

Intermediate Species Detected from $CH_2Cl_2$ Destruction[a]

| | Species | | | | | | | | |
|---|---|---|---|---|---|---|---|---|---|
| Φ | $CCl_2O$ | $C_2HCl_3$ | *cis* 1,2-$C_2H_2Cl_2$ | *trans* 1,2-$C_2H_2Cl_2$ | 1,1-$C_2H_2Cl_2$ | $C_2H_3Cl$ | $C_2H_4$ | $C_2H_2$ | $CH_3Cl$ |
| 0.6 | x | x | x | x | | | | | |
| 0.9 | x | x | x | x | | | | x | |
| 1.0 | x | x | x | x | x | x | | x | |
| 1.1 | | x | x | x | x | x | x | x | x |

[a] An x indicates the presence of a compound for at least one injection temperature.

laboratory [4]; that study examined lean, postflame conditions utilizing a different flow reactor without independent control of equivalence ratio and temperature. Experiments comparing byproducts measured using *in situ* FTIR and *extra situ* sampling to the FTIR long-path-length cell as is used in this study showed that $CCl_2O$ is formed in the reactor, and is not a function of external sampling [41].

The intermediates trichloroethylene ($C_2HCl_3$), *cis*-1,2-dichloroethylene (*cis*-1,2-$C_2H_2Cl_2$), and *trans*-1,2-dichloroethylene (*trans*-1,2-$C_2H_2Cl_2$) follow similar behavior to $CCl_2O$. They also peak in concentration at $T_{inj} \cong 1100$ K, and their concentrations are highest in the leanest experiments. The concentrations of $C_2HCl_3$ and *cis*-1,2-$C_2H_2Cl_2$ are similar, accounting for 5% and 3% of the injected chlorine atoms at $T_{inj} \cong 1100$ K, respectively. The concentrations of *trans*-1,2-$C_2H_2Cl_2$ are lower, accounting for only 1% of the injected chlorine atoms. Most studies in the literature report the total 1,2-$C_2H_2Cl_2$ concentration rather than the separate isomers. The only other study that reported the isomers separately detected them in equal concentrations, with their sum accounting for less than 1% of the injected chlorine [4]. The numerical mechanism does not distinguish between the isomers. The fact that the mechanism does not distinguish between isomers is not expected to greatly affect the predictions of byproducts since the main route is probably isomerization ($E_a$ = 56.9 kcal/mol *trans* ➪ *cis*, $E_a$ = 56.4 kcal/mol *cis* ➪ *trans*) followed by decomposition of *trans*-1,2-$C_2H_2Cl_2$ to chloroacetylene. The structure of *trans*-1,2-$C_2H_2Cl_2$ is more conducive to HCl elimination than *cis*-1,2-$C_2H_2Cl_2$, which could explain the higher concentration of *cis*-1,2-$C_2H_2Cl_2$ detected. Though neither chloroacetylene nor dichloroacetylene were detected in any of the spectra, their formation is not excluded because they are relatively unstable molecules, and could break down in extractive sampling.

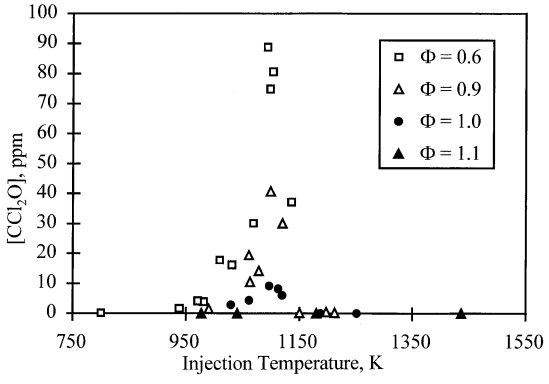


Fig. 4. Phosgene ($CCl_2O$) concentration, residence time ≈ 300 ms. The peak $CCl_2O$ concentration consistently occurs at an $T_{inj} \approx 1100$ K, but is strongly dependent on equivalence ratio.

Figure 5 illustrates how equivalence ratio affects the concentration of several intermediate species at a constant injection temperature of 1075 K. Equal amounts of 1,1- and 1,2-$C_2H_2Cl_2$ are detected in an isothermal flow reactor operating at Φ = 3.0, each accounting for approximately 3% of the injected chlorine atoms [17]. However, the 1,1- and 1,2-isomers of $C_2H_2Cl_2$ detected in the postflame conditions show opposing trends: 1,1-$C_2H_2Cl_2$ increases with equivalence ratio, whereas 1,2-$C_2H_2Cl_2$ decreases (Fig. 5). The nondetection of 1,1-$C_2H_2Cl_2$ at low equivalence ratios agrees with the lean postflame study of Vitovec et al. [4]. Other trends with increasing equivalence ratio are: a sharp decline in $CCl_2O$, a decline in *cis*-1,2-$C_2H_2Cl_2$ between Φ = 0.6 and 0.9, a

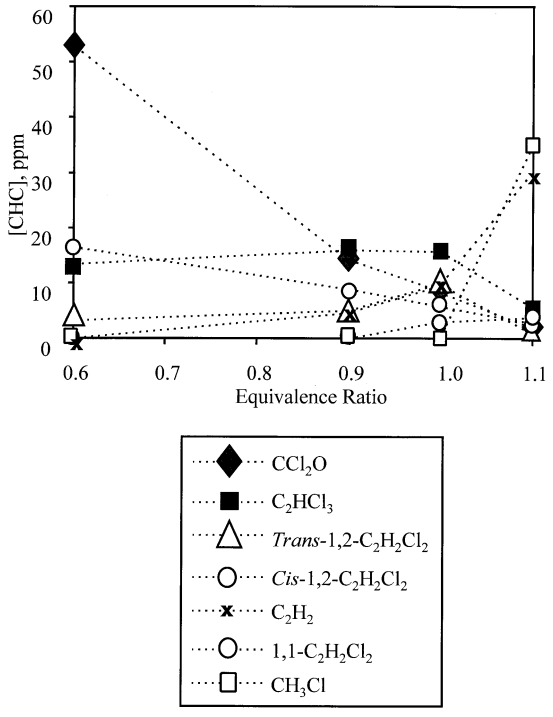


Fig. 5. Comparison of intermediate species detected as a function of equivalence ratio, $T_{inj}$ = 1075 K and residence time ≈ 300 ms. The concentration of $CCl_2O$ exhibits the strongest dependence on equivalence ratio. Byproducts that increase with equivalence ratio: $CHCl_3$, 1,1-$C_2H_2Cl_2$, $C_2H_2$, and $C_2H_4$; byproducts that decrease with equivalence ratio: *Cis*-1,2-$C_2H_2Cl_2$, $C_2HCl_3$, and $CCl_2O$.

decline in $C_2HCl_3$ between Φ = 1.0 and 1.1, a small peak for *trans*-1,2-$C_2H_2Cl_2$ at Φ = 1.0, and sharp increases in acetylene ($C_2H_2$) and $CH_3Cl$ at rich conditions (Φ = 1.1). While not plotted, the concentration of vinyl chloride ($C_2H_3Cl$) follows that of 1,1-$C_2H_2Cl_2$; both species are detected at lower peak concentrations than the other intermediates, and only for Φ = 1.0. Ethylene ($C_2H_4$) and methyl chloride ($CH_3Cl$) are detected only at Φ = 1.1.

Figure 6 displays the combined effects of temperature and equivalence ratio on the chlorinated intermediate species. The observed intermediate species are fully destroyed at temperatures 20–40 degrees higher than for the parent compound; the exception is $C_2H_2$ at Φ = 1.1, which increases with $T_{inj}$ across the range of injection temperatures measured. Holding the equivalence ratio constant, a temperature window (~1100–1150 K) exists for Φ = 1.0 where

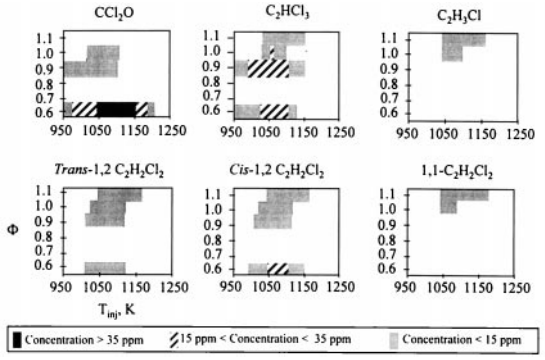


Fig. 6. Concentration of $CCl_2O$ and chlorinated ethylene intermediate species, residence time = 300 ms. Data were collected only for Φ = 0.6, 0.9, 1.0, and 1.1.

the injected $CH_2Cl_2$ is fully destroyed while byproduct concentrations peak. The observation that chlorinated species persist in conditions in which the parent compound is destroyed is consistent with previous findings, especially for $C_2$ species formed from the destruction of $C_1$ species [18, 22, 24]. High destruction efficiencies are achieved without unwanted byproducts at the highest temperatures (>1200 K) for all equivalence ratios tested.

Several byproducts detected are qualitatively consistent with the stable species previously reported (for the same equivalence ratio) in the literature [13, 15, 17, 42]. For instance, the lean (Φ = 0.6) experimental results match well with those of Vitovec et al. [42], as expected since the conditions, residence time, and temperature profile closely match that study, although a different flow reactor is utilized. However, our results are also occasionally discrepant in comparison to previously reported experiments. Aside from the differences in $C_2H_2Cl_2$ concentrations detailed above, there are two other notable discrepancies. $CCl_2O$, detected in Φ = 0.6, 0.9, and 1.0 runs here, is not detected by Ho et al. in their isothermal flow reactor study operating at Φ = 1.0 [13], and $CH_3Cl$ is found at Φ = 1.0 by Ho et al. [13], but is only detected here at Φ = 1.1. In other studies, $CH_3Cl$ is also reported as an intermediate in pyrolytic conditions [15], but not detected at Φ = 3.0 [17]. Some of the pyrolytic products detected by Tavakoli et al. [15] are also formed in the higher equivalence ratio experiments here: $C_2H_2$, and $C_2H_4$ (Φ = 1.0 and 1.1) and $CH_3Cl$ (Φ = 1.1

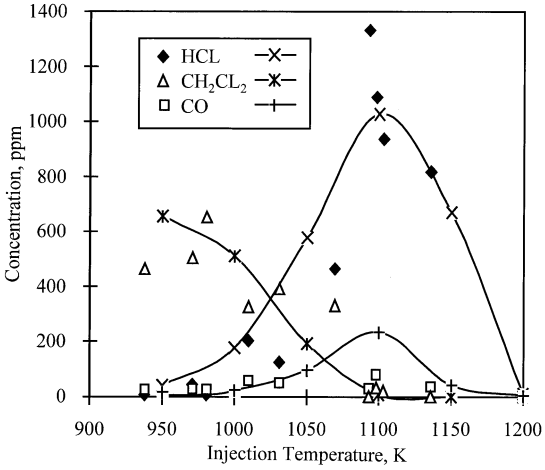


Fig. 7. Major species: numerical predictions (lines) vs. experimental data (symbols), $\Phi = 0.6$, residence time $\approx$ 300 ms. Predicted values compare well with experimental data.

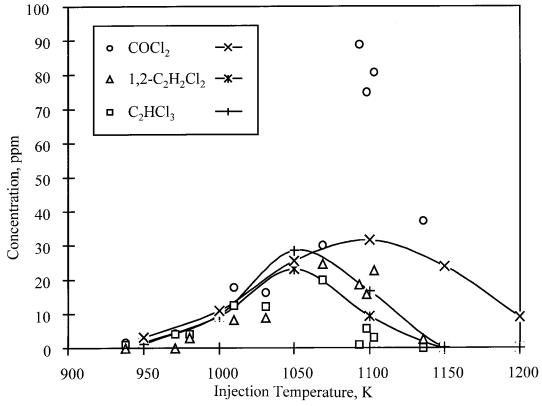


Fig. 8. Minor species: numerical predictions (lines) vs. experimental data (symbols), $\Phi = 0.6$, residence time $\approx$ 300 ms. Predicted values are slightly higher than experimental data for chlorinated ethylenes. However, the concentration of phosgene is underpredicted, and the shape of the curve is relatively smooth compared to the sharp peak detected in experiments at $T_{inj} \approx 1100$ K.

only). However, neither the highly chlorinated species ($C_2Cl_4$ or $CCl_4$) nor the unchlorinated, higher molecular weight species ($C_6H_6$ and $C_2H_6$) formed in pyrolytic conditions are measured in any of the postflame conditions tested. In addition to the species reported, the sample spectra were carefully examined for chlorinated acetylenes, $CH_2O$, $CCl_4$, $C_2Cl_4$, ethane, chlorinated ethanes, and benzene: none were detected. There were no unidentified peaks in the spectra.

## NUMERICAL RESULTS

### Numerical Predictions vs. Experimental Data

The concentrations of major products predicted by the model are plotted in Fig. 7 with the experimental data for $\Phi = 0.6$ and residence times between 294–234 ms. The model predicts HCl and $CH_2Cl_2$ concentrations within experimental error, but CO is overpredicted by a factor of 2. Concentrations of the minor species are plotted in Fig. 8 for $\Phi = 0.6$ and residence times between 294–234 ms. 1,2-$C_2H_2Cl_2$ and $C_2HCl_3$ are predicted within a factor of 2 from their measured values. The model underpredicts $CCl_2O$ by a factor of 3. The experimental data show a relatively sharp peak centered at 1100 K, the temperature at which $CH_2Cl_2$ is fully destroyed, while the code predicts a much broader peak.

Figure 9 compares the predicted byproducts and experimental data for a range of equivalence ratios at a fixed injection temperature of 1075 K. At higher equivalence ratios, the code overpredicts destruction of $CH_2Cl_2$ by a factor of 2, which results in an overprediction of HCl. Most of the measured chlorinated byproducts ($C_2H_3Cl$, $C_2HCl_3$, and 1,2-$C_2H_2Cl_2$) are also overpredicted across the full range of equivalence ratios and temperatures, consistent with an overprediction of $CH_2Cl_2$ destruction. $CH_3Cl$ is overpredicted by a factor of 2 for $\Phi = 1.1$. Approximately 30 ppm $CH_3Cl$ is predicted for $\Phi < 1.1$, but none is detected experimentally (detection limit = 5 ppm). $CCl_2O$ is the only byproduct consistently underpredicted by the code, by a factor of 5 at $\Phi = 0.9$ and by two orders of magnitude at 1.0, where it is measured in trace amounts (<10 ppm). The experiments find increased formation of stable chlorinated organic intermediate species at lower equivalence ratios, while the numerical mechanism predicts the opposite (Fig. 9). This discrepancy is a result of underpredicting $CCl_2O$ while overpredicting $CH_3Cl$.

$C_2H_2$ is overpredicted by the model by an order of magnitude for $\Phi = 0.9$ and 1.0, and by two orders of magnitude for $\Phi = 1.1$ at $T_{inj} =$

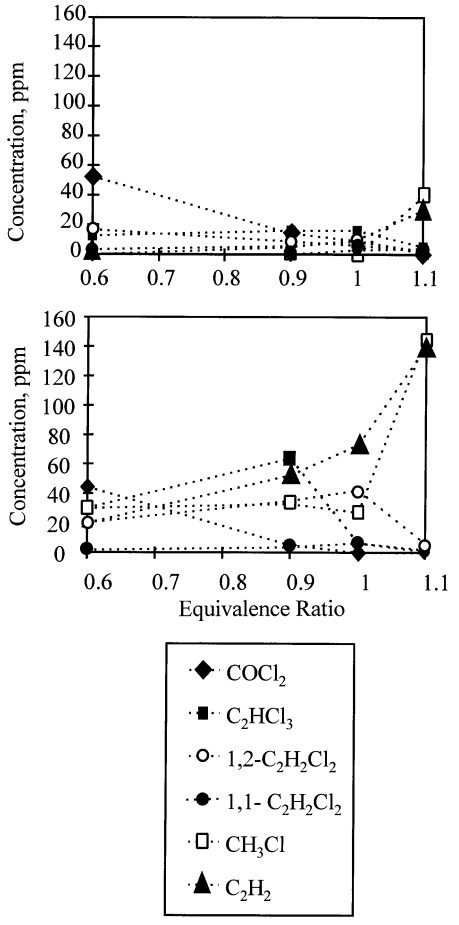


Fig. 9. Experimental measurements (A) and numerical predictions (B) of intermediate species, $T_{inj}$ = 1075 K, residence time = 250 ms. Predictions show increased by-product formation with increasing equivalence ratio while experiments show the opposite trend.

1200 K. $C_2H_4$ is also overpredicted by an order of magnitude for $\Phi = 1.1$. As $C_2H_2$ is a known precursor to higher molecular weight species and soot [43], a possible explanation for its overestimation is that it continues reacting to form higher molecular weight species, and neither the growth reactions nor the higher molecular weight species are included in the mechanism. The absorption spectra were carefully examined for higher molecular weight gaseous species, but none were found. However, trace quantities of soot were deposited on the sample probe during some experiments at $\Phi = 1.0$ and 1.1.

Finally, the model predicts well over 100 ppm of molecular chlorine ($Cl_2$) for the lower equivalence ratios, $\Phi = 0.6$ and $\Phi = 0.9$, and trace amounts (10 ppm) at $\Phi = 1.0$ and $T_{inj}$ = 1200 K. While $Cl_2$ has not been reported in $CH_2Cl_2$ studies, it has been detected in concentrations as high as or higher than HCl for the more highly chlorinated chloroform and carbon tetrachloride at low equivalence ratios [44, 45]. In addition, most studies assume HCl is the main chlorinated product, and calculate its concentration by a chlorine balance rather than directly measuring either HCl or $Cl_2$ [11–13, 25]. Chlorine cannot be measured using IR absorption.

### Important Postflame Reaction Pathways: Reaction Rate Analysis

Reaction rate analysis is used to identify important reaction pathways predicted by the mechanism. Figures 10–12 are reaction pathway diagrams constructed for three equivalence ratios ($\Phi$ = 1.1, 1.0, 0.6) at a midrange injection temperature ($T_{inj}$ = 1000 K). The arrow thickness in these diagrams represents the importance of the route. The numbers, normalized to the amount of $CH_2Cl_2$ destroyed (the only source of chlorine) are the percent chlorine predicted to react through a given route (along arrows) or remain in a stable, chlorinated intermediate (inside boxes). The purpose of this analysis is to map the important pathways predicted by the mechanism to form stable chlorinated species. Therefore, the arrows do not necessarily represent a single, elementary reaction. Instead, chain branching and propagating reactions are combined into one arrow that points directly to the stable species produced. Not all chlorine is explicitly shown on the diagrams. For example HCl removal (not drawn on the diagrams) from $CH_2Cl_2$ forms the CHCl diradical (drawn on the diagrams because it is a major pathway to stable intermediates).

### Destruction of Dichloromethane: Initiation Pathways

Studies of pyrolytic, oxidative pyrolytic, and stoichiometric conditions report that unimolecular decomposition is the most important initiation step for $CH_2Cl_2$ destruction [13, 15, 17]. However, our reaction rate analysis predicts that bimolecular reactions forming $CHCl_2$ are

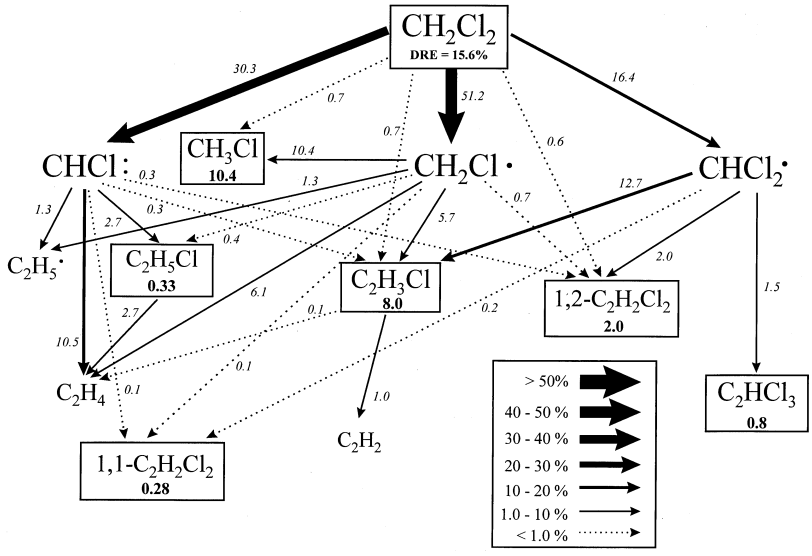


Fig. 10. Reaction pathway diagram, $\Phi = 1.1$, $T_{inj} = 1000$ K, $t_{end} = 0.278$ s. Numbers are the percent chlorine reacting through the channel (arrow) and the percent chlorine remaining in stable species (boxes).

more important for postflame conditions with $\Phi \leq 1.0$. Unimolecular reaction pathways producing $CH_2Cl$ and CHCl are the most important route only for $\Phi = 1.1$. In addition to unimolecular Cl loss, increased amounts of H atoms at $\Phi = 1.1$ opens a bimolecular Cl abstraction pathway, accounting for approximately 10% of $CH_2Cl$ formation at 1000 K. Minor destruction routes exist in which $CH_2Cl_2$ reacts with the CHCl diradical to form either $C_2H_3Cl$ (by subsequent loss of 2 Cl atoms) or 1,2- or 1,1-$C_2H_2Cl_2$ (by HCl elimination). The importance of these routes follows the concentration of CHCl, which is highest at $\Phi = 1.0$ (Fig. 11).

The major shift in destruction reactions occurs between $\Phi = 1.1$ and 1.0 (Figs. 10 and 11). The formation of $CH_2Cl$ is dominant only for $\Phi = 1.1$, while reactions forming $CHCl_2$ dominate for $\Phi = 1.0$. Previous studies discuss possible bimolecular destruction reactions, and show that most available radicals in a CHC combustion environment (Cl, H, OH, O, $H_2O_2$, $HO_2$, and $CH_3$) preferentially abstract H atoms

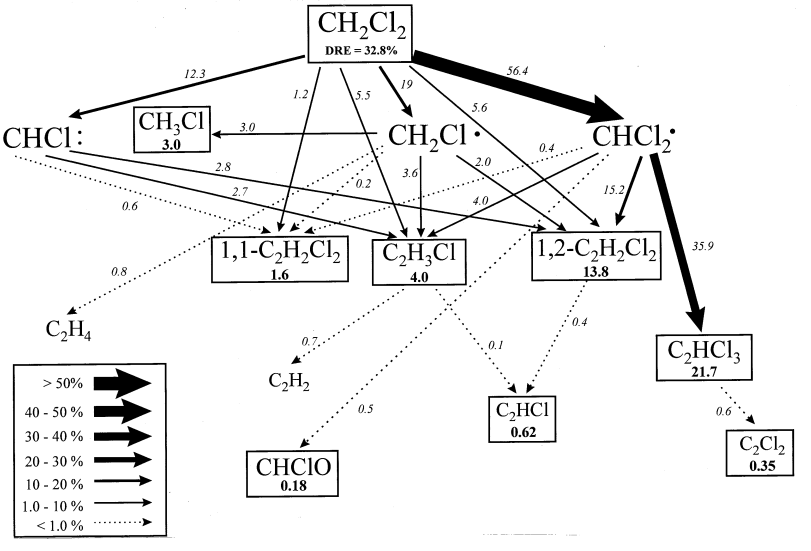


Fig. 11. Reaction pathway diagram, $\Phi = 1.0$, $T_{inj} = 1000$ K, $t_{end} = 0.278$ s. Numbers are the percent chlorine reacting through the channel (arrow) and the percent chlorine remaining in stable species (boxes).

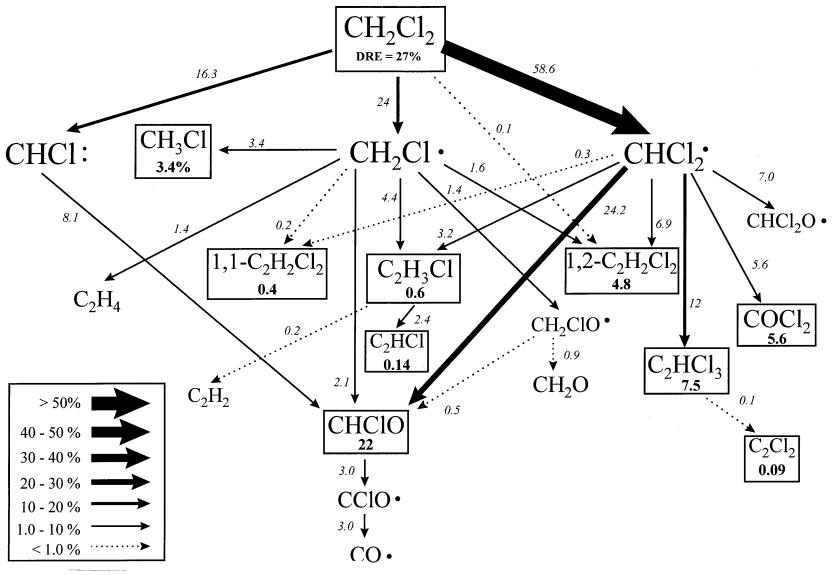


Fig. 12. Reaction pathway diagram, $\Phi = 0.6$, $T_{inj} = 1000$ K, $t_{end} = 0.278$ s. Numbers are the percent chlorine reacting through the channel (arrow) and the percent chlorine remaining in stable species (boxes).

over Cl atoms, forming the dichloromethyl ($CHCl_2$) radical from $CH_2Cl_2$ [13, 24]. Our analysis predicts that H abstraction by Cl is the most important route forming $CHCl_2$ for all equivalence ratios at midrange injection temperature (1000 K). At a high injection temperature (1200 K) and $\Phi = 0.6$, the concentration of OH increases, and its reaction becomes the most important destruction reaction pathway. Though the formation of $CHCl_2$ is not predicted to be the most important destruction pathway in rich conditions ($\Phi = 1.1$), abstraction of H by $CH_3$ radicals opens an additional pathway, accounting for 10% of $CHCl_2$ formation. The relative importance of unimolecular decomposition is less than the bimolecular decomposition of $CH_2Cl_2$ via radical attack for $\Phi = 1.0$, and $CHCl_2$ is preferentially formed.

**Recombination of Chlorinated Radicals: Formation of Stable Intermediates**

Experimentally observed intermediate species, outlined in Table 1, consist mainly of ethylenes ($C_2H_4$, $C_2H_3Cl$, 1,1-and 1,2-$C_2H_2Cl_2$ and $C_2HCl_3$), and the degree of chlorination increases as equivalence ratio decreases. The concentration of $CCl_2O$ also increases with decreasing equivalence ratio. Methyl chloride ($CH_3Cl$) is observed only at $\Phi = 1.1$, and $C_2H_2$ increases with equivalence ratio. The observed shift to more highly chlorinated ethenes and $CCl_2O$ is explained by the recombination of the CHC radicals (CHCl, $CH_2Cl$, and $CHCl_2$) formed at different equivalence ratios (Figs. 10–12). For $\Phi = 1.0$, the dominant destruction route is through bimolecular reactions forming $CHCl_2$, and the importance of this route decreases as equivalence ratio increases. Recombination reactions involving the $CHCl_2$ radical lead to the more highly chlorinated ethylenes observed. Previous studies have shown that $CCl_2O$ can only be formed from a structure with two Cl atoms already bonded to a C atom [20]. Therefore, the concentration of $CCl_2O$ tracks its main precursor, $CHCl_2$. Integrated reaction rate analysis predicts

$$CHCl_2 + ClO = CCl_2O + HCl \quad (1)$$

to be the sole route for $CCl_2O$ formation. Increased $CH_3$ has the effect of forming less chlorinated ethylenes by the following recombination reactions predicted important at $\Phi = 1.1$:

$$CHCl_2 + CH_3 = C_2H_3Cl + HCl \quad (2)$$

$$CH_2Cl + CH_3 = C_2H_4 + HCl. \quad (3)$$

In summary, the relative formation of intermediate species detected from dichloromethane decomposition in postflame conditions can be explained by the difference in relative amounts

of the radicals $CH_2Cl$ and $CHCl_2$, and their recombination. Lean environments create more $CHCl_2$ radicals, greater amounts of $CCl_2O$, and the more highly chlorinated $C_2$ intermediates 1,2-$C_2H_2Cl_2$ and $C_2HCl_3$. In slightly rich conditions, recombination reactions with $CH_3$ open additional pathways for Cl removal and formation of less chlorinated $C_2$ intermediates.

Finally, increasing the injection temperature increases the rate of reaction and promotes more complete conversion to HCl. No appreciable changes in pathways are predicted from changing injection temperature ($T_{inj}$ = 1000 and 1200 K) while holding the equivalence ratio constant ($\Phi$ = 0.6). However, at the higher injection temperature, full destruction of $CH_2Cl_2$ is predicted and relatively much less chlorine is bound in stable intermediate CHCs.

## CONCLUSIONS

Adding excess air to postflame conditions increases destruction of dichloromethane. $CCl_2O$ is the highest yield byproduct detected. The concentrations of $CCl_2O$, $C_2HCl_3$, and 1,2-$C_2H_2Cl_2$ show similar trends with equivalence ratio; their yields increase as equivalence ratio decreases below stoichiometric conditions. In contrast, the concentrations of 1,1-$C_2H_2Cl_2$, the less chlorinated ethylene, $C_2H_3Cl$, and $CH_3Cl$ increase with increasing equivalence ratio. The concentrations of $CCl_2O$, $C_2HCl_3$, and 1,2-$C_2H_2Cl_2$ peak at an injection temperature ($\sim$1100 K) that fully destroys the injected $CH_2Cl_2$.

Comparison of the numerical predictions and experimental data shows reasonable agreement, but a few notable differences remain. For $\Phi >$ 0.6, the code overpredicts $CH_2Cl_2$ destruction, and as a result also overpredicts HCl and chlorinated byproduct formation when compared to experiments. However, $CCl_2O$ is consistently underpredicted across the conditions tested, suggesting either the rate constants for reaction 1 are inaccurate, or additional formation pathways exist that are not accounted for in the mechanism. Finally, $CHCl_3$ is predicted for all equivalence ratios, but only detected in low concentration at $\Phi$ = 1.1.

These results suggest that the oxidative conditions of incinerator postflame regions are best suited to maximize destruction of dichloromethane in the waste fuel, but cooled portions of the flow could promote conversion to chlorinated intermediate species instead of the desired HCl. The postflame conditions modeled could produce $C_2HCl_3$ and $C_2H_2Cl_2$. These two species were both listed among the most frequently detected organics in field tests evaluating emissions from incinerators, industrial boilers, and kilns burning hazardous waste; this field study did not include a detection strategy for $CCl_2O$ [46]. The results of our work suggest that if $C_2HCl_3$ and $C_2H_2Cl_2$ are generated by reactions in postflame conditions during the combustion of hazardous waste, the presence of $CCl_2O$ is also expected. Bimolecular radical attack of $CH_2Cl_2$ by Cl and OH are the most important destruction initiation reactions at lower equivalence ratios, whereas unimolecular reactions are more important at slightly rich conditions. Measurement of the type of CHCs detected in incinerator emissions can provide information about the probable conditions causing unwanted emissions, and lead to appropriate control strategies.

*The authors thank Professor J. W. Bozzelli, New Jersey Institute of Technology, for providing an updated reaction mechanism for dichloromethane, and C. N. Millet, Ecole Centrale, Paris, France, a visiting scholar who conducted the initial experiments for this study. L. A. Sgro thanks D. Stern for carefully reading the manuscript. The work was supported by Grant P42 ES04705 from the National Institute of Environmental Health Sciences, NIH with funding provided by EPA. Its contents are solely the responsibility of the authors and do not necessarily represent the official views of the NIEHS, NIH, or EPA. Lee Anne Sgro has received additional support through the U. C. Toxic Substances Research and Teaching Program, and through the UC Berkeley Dissertation Writing Fellowship.*

## REFERENCES

1. Koshland, C. P., *Twenty-Sixth Symposium (International) on Combustion*, The Combustion Institute, Pittsburgh, 1996, p. 2049.
2. Cleverly, D. H. (1987). *Municipal Waste Combustion*

*Study: Assessment of Health Risks Associated With Municipal Waste Combustion Emissions*, Rep. EPA/530-SW-87-021.
3. Smith, A. H., and Goeden, H. M., *Combust. Sci. Technol*. 74:51 (1990).
4. Vitovec, W., Koshland, C. P., Lucas, D., and Sawyer, R. F., *Combust. Sci. Technol*. 116–117:153–166 (1996).
5. Senser, D. W., Morse, J. S., and Cundy, V. A., *Haz. Waste Haz. Mat*. 2:473–486 (1985).
6. Kramlich, J. C., *Combust. Sci. Technol*. 74:17 (1990).
7. Sacchi, G. F., Procaccini, C., Longwell, J. P., and Sarofim, A. F., *Haz. Waste Haz. Mat*. 13:39–49 (1996).
8. Trenholm, A., Hathaway, R., and Oberacker, D., in *Products of Incomplete Combustion from Hazardous Waste Incinerators*, U.S. EPA, Washington, DC, 1984, pp. 84–95.
9. Linak, W. P., and Wendt, J. O. L., *Prog. Energy Combust. Sci*. 19:145 (1993).
10. Bruce, K. R., Beach, L. O., and Gullet, B. K., *Waste Management* 11:97–102 (1991).
11. Qun, M., and Senkan, S. M., *Haz. Waste Haz. Mat*. 7:55–71 (1990).
12. Senser, D. W., Cundy, V. A., and Morse, J. S., *Combust. Sci. Technol*. 51:209–233 (1987).
13. Ho, W.-P., Barat, R. B., and Bozzelli, J. W., *Combust. Flame* 88:265–295 (1992).
14. Frenklach, M., Hsu, J. P., Miller, D. L., and Matula, R. A., *Combust. Flame* 64:141–155 (1986).
15. Tavakoli, J., Chiang, H. M., and Bozzelli, J. W., *Combust. Sci. Technol*. 101:135 (1994).
16. Taylor, P., and Dellinger, B., *Environ. Sci. Technol*. 22:438 (1988).
17. Taylor, P. H., Dellinger, B., and Tirey, D. A., *Intl. J. Chem. Kin*. 23:1051–1074 (1991).
18. Miller, G. P., Cundy, V. A., Lester, T. W., and Bozzelli, J. W., *Combust. Sci. Technol*. 98:123–136 (1994).
19. Vitovec, W., Higgins, B. S., Lucas, D., Koshland, C. P., and Sawyer, R. F. (1994). Western States Section/The Combustion Institute, University of California, Davis.
20. Thomson, M. J., Higgins, B. S., Lucas, D., Koshland, C. P., and Sawyer, R. F., *Combust. Flame* 98:350–360 (1994).
21. Koshland, C. P., Fisher, E. M., and Lucas, D., *Combust. Sci. Technol*. 82:49–65 (1992).
22. Fisher, E. M., and Koshland, C. P., *Combust. Sci. Technol*. 85:313–325 (1992).
23. Fisher, E. M., and Koshland, C. P., *Combust. Flame* 90:185–195 (1992).
24. Qun, M., and Senkan, S. M., *Combust. Sci. Technol*. 101:103 (1994).
25. Cundy, V. A., Morse, J. S., and Senser, D. W., *JAPCA* 36:824–828 (1986).
26. Oppelt, E. T., *Tox. Indust. Health* 6:23–51 (1990).
27. Higgins, B. S. (1995). Ph.D. thesis, Dept. of Mechanical Engineering, University of California, Berkeley.
28. Dempsey, C. R., and Oppelt, E. T., *Air Waste* 43:25–73 (1993).
29. Sgro, L. A., Higgins, B. S., et al. (1995). *Numerical Characterization of a Vertical Combustion Flow Reactor*. Combustion Fundamentals and Applications, The Central and Western States (USA) Sections and Mexican National Section of the International Combustion Institute and American Flame and Research Committee, San Antonio, TX, The Combustion Institute.
30. Hall, M. J., Lucas, D., and Koshland, C. P., *Environ. Sci. Technol*. 25:260–269 (1991).
31. Chen, J.-Y., Personal communication, 1997.
32. Kee, R. J., Miller, J. A., and Jefferson, T. H. (1980). *CHEMKIN: A General-Purpose, Problem-Independent Transportable, FORTRAN Chemical Kinetics Code Package*. Sandia National Laboratories Rep. SAND80-8003.
33. Ho, W., Yu, Q.-R., and Bozzelli, J. W., *Combust. Sci. Technol*. 85:23 (1992).
34. Ho, W., and Bozzelli, J. W., in *Twenty-Fourth Symposium (International) on Combustion/The Combustion Institute*, The Combustion Institute, 1992, pp. 743–748.
35. Bozzelli, J. W., Personal communication, 1998.
36. Chiang, H.-M. (1995). Ph.D. thesis, Dept. of Chemical Engineering and Environmental Science, New Jersey Institute of Technology, Newark, NJ.
37. Gargurevich, I. A., Castaldi, M., and Senkan, S. M., *Combust. Sci. Technol*. 106:69–82 (1995).
38. Roesler, J. F., Yetter, R. A., and Dryer, F. L., *Combust. Sci. Technol*. 85:1 (1992).
39. Roesler, J. F., Yetter, R. A., and Dryer, F. L., *Combust. Sci. Technol*. 82:87–100 (1992).
40. Chang, W. D., and Senkan, S. M., *Combust. Sci. Technol*. 43:49–66 (1985).
41. Thomson, M. J., Higgins, B. S., et al., *Combust. Flame* 98:350–360 (1994).
42. Vitovec, W., Higgins, B. S., Koshland, C. P., Lucas, D., and Sawyer, R. F. (1995). *3rd Asia Pacific International Symposium on Combustion and Energy Utilization*, Hong Kong.
43. Goldanskii, V. I., Schafer, F. P., and Toennies, J. P., in *Soot Formation in Combustion* (H. Bockhorn, Ed.), Springer-Verlag, Heidelberg, 1994.
44. Lou, L. C., and Chang, Y. S., *Combust. Flame* 109:188–197 (1997).
45. Lou, J. C., and Chou, Z. H., *Haz. Waste Haz. Mat*. 13:399–407 (1996).
46. EPA, U.S., *Fed. Register* 56:42504–42517 (1991).

*Received 23 December 1998; revised 30 July 1999; accepted 17 August 1999 AQ1: Au: OK with change?*